Shell model molecular dynamics calculations of the Raman spectra of molten NaI

1989 J. Phys.: Condens. Matter 1 2427

(http://iopscience.iop.org/0953-8984/1/13/014)

J. Phys.: Condens. Matter **1** (1989) 2427–2440. Printed in the UK

Shell model molecular dynamics calculations of the Raman spectra of molten NaI

J A Board† and R J Elliott‡
Department of Theoretical Physics, University of Oxford, 1 Keble Road, Oxford OX1 3NP, UK

Received 12 August 1988

Abstract. The shell model used in lattice dynamics is applied to construct an interionic potential for use in molecular dynamics (MD) simulations of molten NaI. The ion shell–core displacements generated by the shell model potentials are used as an approximation to the instantaneous dipole moments of the ions. Time correlation functions of aggregates of these instantaneous ionic dipoles are related to the polarised and depolarised Raman spectra of the melt; fair agreement between simulated and experimentally observed spectra is obtained, indicating that the dipole–induced-dipole mechanism is an important component but not the exclusive contributor to the Raman polarisability in ionic melts.

1. Introduction

1.1. Raman scattering from alkali halides

The Raman spectra of alkali halide crystals have been the subject of a number of theoretical investigations; ionic melts have received less attention. Recent experimental measurements of the Raman spectra of molten salts (Mitchell and Raptis 1983, Raptis *et al* 1983, McGreevy 1987, Giergiel *et al* 1984) have given new impetus to the search for understanding of the scattering mechanisms at work in the melts.

Karo and Hardy (1966) developed an understanding of the Raman spectra of ionic solids through detailed consideration of the two-phonon density of states in these crystals; this led to reasonable explanations for the main features of the crystal spectra but not the intensity of the scattering. Bruce and Cowley (Bruce and Cowley 1972, Bruce 1972) calculated the expected Raman scattering from ionic crystals based on a parametrisation of polarizability tensors in terms of shell model interionic potentials (described below). Neither of these approaches is directly appropriate for studies of melts.

Elliott and Dixon (1981) employed molecular dynamics computer simulation and a simple model for quadrupolar electronic distortions to estimate the light scattering lineshape of molten NaI. Their work indicated that quadrupolar contributions, while probably important, are insufficient to account for light scattering from molten salts.

Madden and Board (1987) have considered a model for the Raman scattering from NaCl crystals and melts based on computer simulation and a detailed consideration of the effects of the instantaneous local ion environment on ionic polarisability. Their

† Present address: Department of Electrical Engineering, Duke University, Durham NC 27706, USA.
‡ To whom all correspondence should be addressed.

0953-8984/89/132427 + 14 $02.50

approach does give some understanding of the intensity, as well as the lineshape, of the scattering, but it requires detailed information about the variation of the electronic structure of the constituent ions under environment fluctuations in order to parametrise the polarisability models.

The current work takes a new approach. Through explicit calculation of instantaneous ion dipole moments in a computer simulation, dynamical dipole moment fluctuations are related to expected light scattering lineshapes.

1.2. Molecular dynamics and shell model potentials

Molecular dynamics simulation (MD) is now a well established computational technique for exploring the dynamics and statics of atomic systems (Hoover 1986, Ciccotti and Hoover 1987). In its simplest form, MD involves integrating the Newtonian equations of motion for a set of particles obeying some force law, thereby obtaining the phase space trajectories of these particles. Properties of interest are calculated from the record of these trajectories.

Dixon and Sangster (1975, 1976) developed the use of *polarisable ion*, or *shell model* interionic potentials based on the shell model of lattice dynamics (Cochran and Cowley 1967) in MD simulations of molten alkali halide systems. Simpler *rigid-ion model* potentials (Sangster and Dixon 1976), in which ions are modelled as rigid, massive, point-charged particles, had been shown to be inadequate to reproduce the proper lattice dynamics of many alkali halide crystals. The shell model potentials treat ions as massive, charged, rigid, point ion cores surrounded by and attached via harmonic springs to massless, charged, outer electron 'shells'. This model allows for crude incorporation of the effect of ionic polarisability on the short-range interactions between ions as their local environments change dynamically; proper modelling of crystal lattice dynamics is possible with these models for most alkali halides. The use of potentials based on shell model potentials in melts is expected also to give better estimates of dynamical properties than rigid-ion simulations, although static properties, such as pair-correlation functions, are modelled more or less equally well by rigid- and shell model potentials in melts. Sangster and Dixon (1976) describe the MD methods and the potential model used in this work in detail.

The present study focuses on molten NaI. This salt is one for which the use of shell-model potentials is particularly necessary to obtain good phonon properties in the crystal, so it is expected that any benefits from going to the extra computational expense (about a factor of 10) of using shell-model potentials as opposed to rigid ion ones in MD calculations will be maximum here. NaI has the additional attraction that only the highly polarisable iodine ion need be modelled by a shell-core combination; the sodium ion can be treated as rigid, as it is nearly unpolarisable. This results in a great savings in computing costs. The shell model potential used in this work is known to reproduce the low-temperature phonon dispersion relations for NaI quite accurately, whereas rigid ion potentials must, by construction, fail dramatically (Dixon and Sangster 1976).

As a result of performing shell model simulations of a salt such as NaI, the coordinates for both the ion cores and their electron shells (for the anions) are available for each ion at each timestep. The difference of these two for a given ion i is that ion's instantaneous fluctuating electronic dipole moment μ_i within the approximations of the shell model. Note that this is not the same as the *induced* dipole moment π_i, since there is no external field present in the simulation to cause any induction. μ_i is the result of local, instantaneous electric field fluctuations within the sample as well as short-range inter-

actions with neighbouring ions. This work seeks to take advantage of the extra data, beyond that which the rigid-ion potential simulations can provide, in the formation of calculable models for ion properties, specifically light scattering. Comparison with experiment should indicate whether or not this calculated dipole moment is a reasonable representation of the 'real' dipole moment, or simply an unphysical artefact of the simulation method.

1.3. Terminology for scattering from melts

There is some confusion in the literature as to the termnology appropriate for the light scattering in melts. What is referred to here as 'Raman scattering' from these ionic systems is equivalently termed 'depolarised Rayleigh scattering' (the usual term in work on argon, since the polarised spectrum is simply $\frac{4}{3}$ times the depolarised spectrum), or perhaps most appropriately, 'Rayleigh wing scattering' (Clarke 1978). Some workers reserve the term 'Raman scattering' in liquids work for scattering from intramolecular degrees of freedom; for ionic systems, this distinction is irrelevant.

2. Theory of Raman scattering

2.1. Standard model for induced dipole scattering

The usual treatment of light scattering in liquids (Clarke 1978) proceeds from the calculation of transition rates for processes involving the spontaneous emission of a photon from a system excited by the presence of an induced dipole moment

$$\mathcal{M}(t) = \sum_i \pi_i(t).$$

If the scattered radiation with polarisation $\boldsymbol{n}_s$ is measured in a direction perpendicular to the incident radiation, then the scattered Stokes intensity $I(\omega)$ at frequency shift ω is given by (Clarke 1978)

$$I(\omega) \simeq \sum_{i,f} \rho_i |\langle f|\mathcal{M} \cdot \boldsymbol{n}_s|i\rangle|^2 \delta(\omega - \omega_{if}). \tag{1}$$

Here ω_{if} is the frequency corresponding to the difference in energies of the initial state $|i\rangle$ and the final state $|f\rangle$ of the liquid. The incident radiation is at frequency ω_0. The 'constant' of proportionality contains factors in $(\omega_0 - \omega)^4$ (but $\omega \ll \omega_0$ so these are effectively constant over the frequency range of interest) and a *local* field *correction factor*, which corrects for the difference between the radiation field in the sample and the applied field (Clarke 1978). Polarised scattering results when $\boldsymbol{n}_s$ is parallel to $\boldsymbol{n}_0$, the polarisation of the incident field; depolarised scattering occurs when $\boldsymbol{n}_s$ is perpendicular to $\boldsymbol{n}_0$.

Clarke (1978) transforms (1) from the Schrödinger representation, where the states are time-dependent, to the Heisenberg representation, where the time dependence is in the operator $\mathcal{M}(t)$. The Stokes intensity $I(\omega)$ is shown to be dependent on the Fourier transform of the time correlation function of the dipole operator $\mathcal{M}(t)$:

$$I(\omega) \simeq \int_{-\infty}^{\infty} dt\, e^{-i\omega t} \langle \mathcal{M}(0)\mathcal{M}(t)\rangle. \tag{2}$$

This model is not useful to the current simulation work, however, since it depends

on the induced dipoles π_i; this data is not available from simulations at present. The simulations do, however, give information about the thermally fluctuating electronic dipoles μ_i. The standard model gives an indication of how to proceed in order to develop a calculable model based on μ_i instead of π_i.

2.2. *A second-order treatment*

The model above disregards the absorption of the incident photon as the origin of the induced dipole $\mathcal{M}$, and thus ignores the second-order (in the electron–photon interaction) nature of the Raman transitions. To treat this aspect of the scattering more accurately, a reduction to time correlation functions is here performed on the second-order Raman transition probability expression. The model so derived will be calculable in terms of the available simulation data.

The second-order (in the electron-photon interaction) quantum transition probability for Raman processes mediated by an interaction Hamiltonian $\mathcal{H}_{\text{int}}$ is given by (Placzek 1934, Birman 1974)

$$\omega_{\text{I}\to\text{F}} = \left|\frac{\Sigma_{\text{EX}}\langle\text{F}|\mathcal{H}_{\text{int}}|\text{EX}\rangle\langle\text{EX}|\mathcal{H}_{\text{int}}|\text{I}\rangle}{E_{\text{I}} - E_{\text{EX}}}\right|^2 \delta(E_{\text{I}} - E_{\text{F}}). \tag{3}$$

This is the probability of a Raman-type transition from initial state $|\text{I}\rangle$ to an energy conserving final state $|\text{F}\rangle$, mediated by an intermediate excited electronic state $|\text{EX}\rangle$. The states $|\text{I}\rangle$ and $|\text{F}\rangle$ here are states of the whole system, liquid plus photons. Placzek's approximation that the electrons are in their ground states before and after the scattering is in force, so the energy shift $\hbar\omega$ of the scattered photon of frequency ω_{S} from the incident laser photon frequency ω_{L} represents a gain or loss of energy by the excitations of the sample (referred to as 'phonons' though in a liquid they are not harmonic vibrations).

To make the frequency dependence of the scattering more explicit, we use the states $|\text{i}\rangle$ and $|\text{f}\rangle$ defined for the matter system only (electron-phonon states) and leave changes of the photon states as implied. Now the delta function in (3) can look like that in (1): for scattering at a frequency shift of ω

$$\omega_{\text{i}\to\text{f}} = \left|\frac{\Sigma_{\text{EX}}\langle\text{f}|\mathcal{H}_{\text{int}}|\text{EX}\rangle\langle\text{EX}|\mathcal{H}_{\text{int}}|\text{i}\rangle}{E_{\text{i}} - E_{\text{EX}}}\right|^2 \delta(\omega - \omega_{\text{if}}). \tag{4}$$

The difference in the energy of the initial and final matter states, $\hbar\omega_{\text{if}}$, must be the same as the energy imparted to or from the scattered photon, $\hbar\omega$.

The total probability of Stokes scattering processes at a frequency shifted by ω from the incident frequency is found by taking a Boltzmann weighted sum of (4) over all initial states $|\text{i}\rangle$, and a sum over all energy conserving final states $|\text{f}\rangle$, so that

$$P(\omega) = \sum_{\text{i,f}} \rho_i \left|\frac{\Sigma_{\text{RX}}\langle\text{f}|\mathcal{H}_{\text{int}}|\text{EX}\rangle\langle\text{EX}|\mathcal{H}_{\text{int}}|\text{i}\rangle}{E_{\text{i}} - E_{\text{EX}}}\right|^2 \delta(\omega - \omega_{\text{if}}). \tag{5}$$

The scattering intensity $I(\omega)$ will be proportional to $P(\omega)$ if the shifts ω are small when compared with ω_0.

This expression is not useful for MD work, as there is no knowledge of intermediate excited electronic states in these MD calculations. The explicit treatment of the intermediate excited state $|\text{EX}\rangle$, and the separate inclusion of the incident and scattered photons, are the differences between this expression and (2) above. The excited state is a manifestation of the induced dipole moment of (2), but its origin is clearer here.

In the spirit of the shell model, it is asserted that there is *one dominant, excited electronic state* $|E\rangle$ in the system. This is equivalent to a harmonic shell-core restoring force with a single frequency for shell-core oscillations; all polarisability effects are represented through one process. In lieu of the sum over all excited states $|EX\rangle$, an 'average energy denominator' $\Delta E = E_i - E_E$ is introduced, and the sum over $|EX\rangle$ is reduced to a projection into the single state $|E\rangle$. Removing the (now constant) projection into $|E\rangle$, and substituting the dipole approximation representation (Birman 1974, Bilz *et al* 1984) of the interaction Hamiltonian $\mathcal{H}_{int}$, the scattering intensity can be rewritten as

$$I(\omega) \simeq \frac{1}{\Delta E} \sum_{i,f} \rho_i \left| \langle f| \left(\sum_{j,\beta} E^j_{S,\beta} \mu^j_\beta \right) \left(\sum_{i,\alpha} E^i_{L,\alpha} \mu^i_\alpha \right) |i\rangle \right|^2 \delta(\omega - \omega_{if}) \tag{6}$$

where E^i_L is the incident laser field on ion i; E^j_S is the scattered field acting on ion j, and μ^i is the instantaneous dipole moment of ion i. Note that μ is simply the instantaneous electronic dipole moment; its origin (i.e., via external field induction or not) is irrelevant. The incident laser field interaction mediates the transition from the initial state $|i\rangle$ to the (now fixed) intermediate state; the scattered field is involved in the transition to the final state $|f\rangle$.

The electric fields in this expression are non-interacting; the effect of the fields in a melt (where ion positions and dipole orientations are random to some approximation) can be captured by averaging over all field directions and lumping the result into a constant prefactor, which is dropped, leaving

$$I(\omega) \simeq \sum_{i,f} \rho_i \sum_{\alpha\beta} |\langle f|M_\beta M_\alpha|i\rangle|^2 \delta(\omega - \omega_{if}) \tag{7}$$

where

$$M = \sum_i \mu^i.$$

Transforming (7) to the Heisenberg representation gives

$$I(\omega) \simeq \int_{-\infty}^{\infty} dt\, e^{-i\omega t} \sum_{i,f} \rho_i \sum_{\alpha\beta} \langle i|M_\beta(0)M_\alpha(0)|f\rangle\langle f|M_\beta(t)M_\alpha(t)|i\rangle. \tag{8}$$

Performing the central sum over states $|f\rangle$ (which are assumed to be a complete set, thus $\Sigma_f|f\rangle\langle f| = 1$), the scattering intensity is now

$$I(\omega) \simeq \int_{-\infty}^{\infty} dt\, e^{-i\omega t} \sum_{i} \rho_i \sum_{\alpha\beta} \langle i|M_\beta(0)M_\alpha(0)M_\beta(t)M_\alpha(t)|i\rangle. \tag{9}$$

This expression, involving the sum over states $|i\rangle$ weighted by their Boltzmann factors ρ_i, is the Fourier transform of the thermal average of the four dipole operator:

$$I(\omega) \simeq \int_{-\infty}^{\infty} dt\, e^{-i\omega t} \sum_{\alpha\beta} \langle M_\beta(0)M_\alpha(0)M_\beta(t)M_\alpha(t)\rangle_T \tag{10}$$

where $\langle \ldots \rangle_T$ denotes the equilibrium thermal average. The ensemble average is given by the corresponding time correlation function (Clarke 1978), so finally for the scattering intensity $I(\omega)$

$$I(\omega) \simeq \int_{-\infty}^{\infty} dt\, e^{-i\omega t} \sum_{\alpha\beta} \langle M_\beta(0)M_\alpha(0)M_\beta(t)M_\alpha(t)\rangle. \tag{11}$$

Table 1. Potential parameters for shell model simulation of NaI. The interionic potential is of the form

$$\Phi_{\alpha\beta}(r) = Z_\alpha Z_\beta \frac{e^2}{r} + B_{\alpha\beta} \exp\left(-\frac{r}{\sigma_{\alpha\beta}}\right) - \frac{C_{\alpha\beta}}{r^6} - \frac{D_{\alpha\beta}}{r^8}$$

for ions of type α and β (each cation or anion) with ionic charge Z_α and Z_β separated by a distance r. The sodium ion has a charge $Z_+ = 1$ (in units of e); the iodine ion has core charge $2.045e$ and shell charge $-3.045e$ for a net charge of -1. The spring constant per unit cell volume for the anion shell is 1.312 Å^{-3}. From Dixon and Sangster (1976).

	+ +	+ −	− −
B (10^{-12} erg)	1753.3	2884.7	4449.5
C (10^{-12} erg Å^6)	1.68	19.1	392.0
D (10^{-12} erg Å^8)	0.8	31.0	1100
σ (Å^{-1})	0.3427	0.3427	0.3427

The expression (11) means that the probability of a Raman event involving an emission of a photon of frequency $(\omega_0 - \omega)$, that is, shifted by ω from the incident frequency, is proportional to the Fourier transform of the time correlation of the dipole product $M_\alpha(t)M_\beta(t)$. There are two distinct types of scattering events to consider, those with $\alpha = \beta$, and those with $\alpha \neq \beta$. An example of the first type of event is when $\alpha = \beta = x$: this corresponds to a *polarised* scattering event, since the dipole moments involved at the incident and scattering events are in the same direction. An example of the second type of event is when $\alpha = x$ and $\beta = y$; this corresponds to a *depolarised* scattering event, since orthogonal polarisation components are involved. Thus

$$I_\parallel(\omega) \simeq \int_{-\infty}^{\infty} dt\, e^{-i\omega t} \sum_\alpha \langle M_\alpha(0)M_\alpha(0)M_\alpha(t)M_\alpha(t)\rangle \tag{12}$$

$$I_\perp(\omega) \simeq \int_{-\infty}^{\infty} dt\, e^{-i\omega t} \sum_{\alpha\neq\beta} \langle M_\beta(0)M_\alpha(0)M_\beta(t)M_\alpha(t)\rangle. \tag{13}$$

Although the scattering intensities given by these expressions are in arbitrary units, their relative values should be consistent, so the ratio of $I_\perp$ to $I_\parallel$ should give the frequency-dependent depolarisation ratio $\rho(\omega)$:

$$\rho_D(\omega) = \frac{I_\perp(\omega)}{I_\parallel(\omega)}. \tag{14}$$

The integrated depolarisation ratio ρ_D is available from the $t = 0$ values of the correlation functions in (12) and (13) (Fairbanks *et al* 1986).

3. Results

3.1. Calculations on NaI

The above model has been tested on a shell model simulation of 216 ions of molten NaI at 973 K; the potential parameters used are those of Dixon and Sangster (1976); they are given in table 1. Usual microcanonical MD techniques were employed; no constraints were applied to the temperature or pressure. The simulation employed a timestep of 0.5348×10^{-14} s and was run for 10000 timesteps on the IBM 3081 system at the

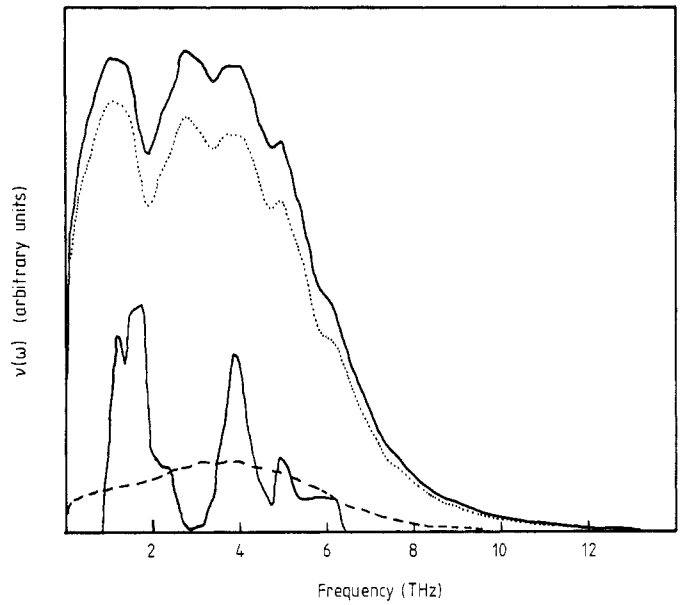

Figure 1. Spectral function $\nu(\omega)$ calculated from (15) for simulation of 216 ions of molten NaI at 973 K. In a crystal, this would be the one-phonon density of states. The total excitation spectrum is given by the upper full curve. The excitations for cations are given by the broken curve; anion excitations are given by the dotted curve. The total crystal density of states, as calculated from a simulation at 100 K, is also given by the lower full curve (at arbitrary relative intensity) for comparison. The gap in this at low ω is due to bad statistics in this region.

Rutherford Appleton Laboratory. Approximately 100 hours of CPU time were required for this simulation and its analysis.

Simulations performed in this manner are known to yield good results for the melt structure and such properties as the ion-diffusion constants (Dixon and Sangster 1976). Extensive studies of neutron scattering and other dynamical properties of molten NaI have been undertaken with the same methods and potential model (Dixon 1983a, b, c).

Proper representation of vibrational modes is particularly important in a calculation of Raman scattering. A simulation of NaI at 100 K was performed with the same potential model and MD methods, and the one-phonon density of states $\nu(\omega)$ was calculated from the velocity autocorrelation function (Elliott *et al* 1974)

$$\int_0^\infty \sum_i m_i \langle v_i(0) v_i(t) \rangle \, \mathrm{e}^{-\mathrm{i}\omega t} \, \mathrm{d}t = \omega n(\omega) \nu(\omega) \tag{15}$$

where the sum is over ions i with masses m_i and $n(\omega)$ is the Bose–Einstein weighting factor. This yielded a one-phonon density of states in excellent agreement with that expected from the phonon-dispersion relations for the potential model used, as given by Dixon and Sangster (1976). Crystal simulations at higher temperatures produced a broadening and shifting of the phonon density of states that was consistent with lattice dynamics calculations of the potential dispersion relations at lattice parameters appropriate to the higher temperatures. The simulation method is therefore thought to provide a realistic representation of the vibrational modes in the system.

For the melt simulations, the spectral function equivalent to the one-phonon density of states $\nu(\omega)$ in the crystal (15) was calculated; the results are given in figure 1, where

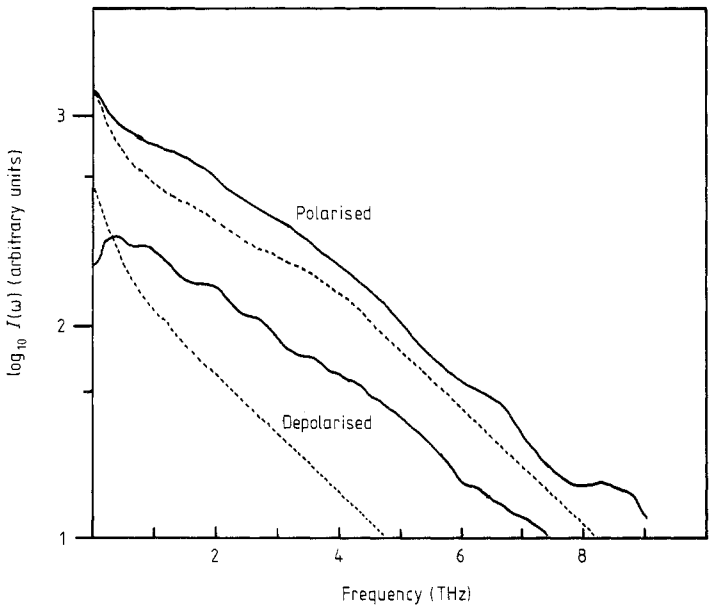

Figure 2. Smoothed semi-log plot of the polarised and depolarised scattering as given by (12) and (13) for a 216 ion simulation of molten NaI with shell model potential at 973 K, compared with the experimental results of Raptis *et al* (1983) (dotted curves). The two polarised curves have been normalised to the same arbitrary intensity at $\omega = 0$; the depolarised curves are plotted at their known relative intensities with respect to the polarised curves. The time correlation functions giving rise to these curves are given in figure 3; the unsmoothed version of these curves is given in figure 4.

the crystal result (calculated from a similar simulation at 100 K) is also plotted for comparison. These results show that the excitation spectra of the liquid are broader than but not dramatically different from the one-phonon spectrum of high-temperature crystals, indicating that significant phonon-like excitations persist in the melt.

3.2. Experimental data

Recent Raman measurements of most of the alkali halide melts have been performed by Mitchell *et al* (1983) (also Raptis *et al* 1983, McGreevy 1987), and by Giergiel *et al* (1984). Both groups have measured $I_{\parallel}(\omega)$ and $I_{\perp}(\omega)$ for molten NaI, and the former have given $\rho_D(\omega)$. The two groups are in close agreement on most details of their measurements; this will permit reliable comparison of the results from the model calculation with experiment.

The experimental intensities of Raptis *et al* (1983) for NaI at 968 K are given by the broken curves on a semi-log scale in figure 2. The results of Giergiel *et al* (1984) are very similar. Both the polarised and depolarised spectra are characterised by long, high-frequency exponential (straight lines in figure 2). The polarised spectrum has a pronounced shoulder at about 4 THz, marking a transition to a more complex low-frequency behaviour. a second exponential with a different decay constant can characterise the lineshape between about 1 and 4 THz; Raptis *et al* (1983) claim the low-frequency region up to about 1 THz is also exponential in character with yet another characteristic decay, although this is less clear from the figure. The depolarised spectrum also has complex behaviour below about 1 THz, but a single exponential characterizes the high-frequency

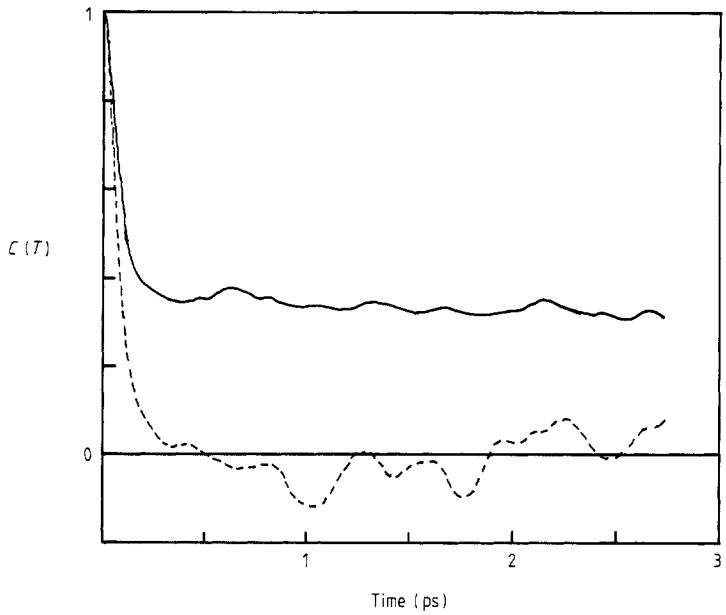

Figure 3. Time correlation functions $c(t)$ from the simulation whose Fourier transforms in (12) and (13) give the Raman spectra in figure 2. The full curve gives rise to the polarised scattering, the broken curve to depolarised scattering. The long-time average value of the polarised curve must be subtracted off and its amplitude rescaled prior to taking the Fourier transform.

portion; there is no shoulder here.

The exponential decays of the various regions of the spectra have been characterised (Raptis *et al* 1983) by time constants τ_s with $\tau_s = 1/\omega_s$ (ω_s in THz), and

$$I(\omega) = I_0 \, e^{-\omega/\omega_s}. \tag{16}$$

3.3. Data analysis

Plots of the calculated lineshapes $I_\perp(\omega)$ and $I_\parallel(\omega)$ from a simulation using the shell model potential are given by the full curves on a semi-log scale in figure 2 where they are compared with experiment.

The determination of the depolarised spectra is straightforward; the time correlation function (13) is well behaved in that it decays to zero fairly rapidly, and taking its Fourier transform presents no problems (broken curve in figure 3). The polarised correlation function (12), however, has a non-zero long-time value (full curve in figure 3) since it is the product of two squares. The long-time average value must be subtracted off and the amplitude rescaled before taking the Fourier transform. As the time spectra are quite noisy, the best value of this long-time average is a subjective judgment, but the resulting spectra were found not to be very sensitive to small changes in the value of this long-time average.

The spectra in figure 2 have been smoothed through the application of a low-pass filter to reduce the statistical noise that is the result of the relatively short length of the simulation run. This simulation was equilibrated for 5000 timesteps, and the data was collected over the next 5000 timesteps. An independent simulation run with a slightly modified potential produced largely equivalent results, giving confidence in the filtering procedure. Figure 4 gives an example of the unsmoothed spectra used to generate figure 2.

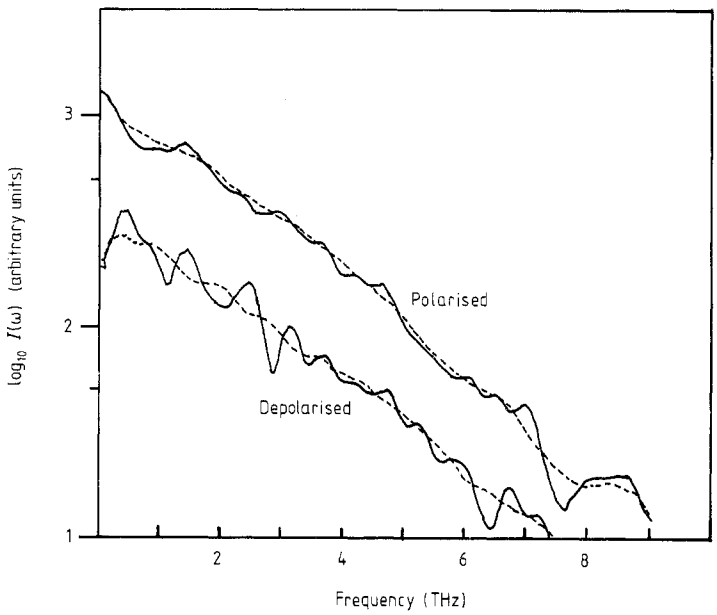

Figure 4. Semi-log plots of the unsmoothed Fourier transforms of the time correlation functions for the simulation in figure 3. The smoothed versions of these curves (broken curves) from a low-pass filtering operation are the polarised and depolarised spectra of figure 2.

Table 2. Scattering intensities and depolarisation ratios. The integrated polarised $I_{\parallel}$ and depolarised $I_{\perp}$ intensities from simulation (note: arbitrary units) and experiment (units above) give the total (integrated) depolarisation ratio ρ_D. Giergiel *et al* (1984) did not report absolute intensities. The low-frequency ($\rho_D(0)$) and high-frequency ($\rho_D(\infty)$) limits as extrapolated from figure 2 are also given.

	Simulation	Raptis *et al* (1983) Fairbanks *et al* (1986)	Giergiel *et al* (1984)
$I_{\perp}$	135 (arb)	1.46×10^{-29} (cm^2 sr^{-1} ion pair^{-1})	—
$I_{\parallel}$	446 (arb)	6.65×10^{-29} (cm^2 sr^{-1} ion pair^{-1})	—
ρ_D	0.30	0.219	—
$\rho_D(0)$	0.3	0.34	0.3
$\rho_D(\infty)$	0.3	0.11	0.125

3.4. Scattering intensities and depolarisation ratios

The absolute scattering intensity is not reliable from this model, since the shell charges and masses are not defined to produce an absolute value of the dipole moments. For this reason the prefactors of the intensity expressions (12) and (13) were not determined. The polarised and depolarised spectra are calculated in the same way, however, so the relative intensity of the two is more valid. Specifically, the integrated intensities are related to the $t = 0$ values of the time correlation functions in (12) and (13); the total (integrated) depolarisation ratio for the model is therefore available. The frequency-dependent depolarisation ratio $\rho_D(\omega)$ can be determined from the ratio of the curves in figure 2. These quantities are also available experimentally; the results are summarised in table 2. Figure 5 gives $\rho_D(\omega)$ for the simulation and experiment. The low-frequency

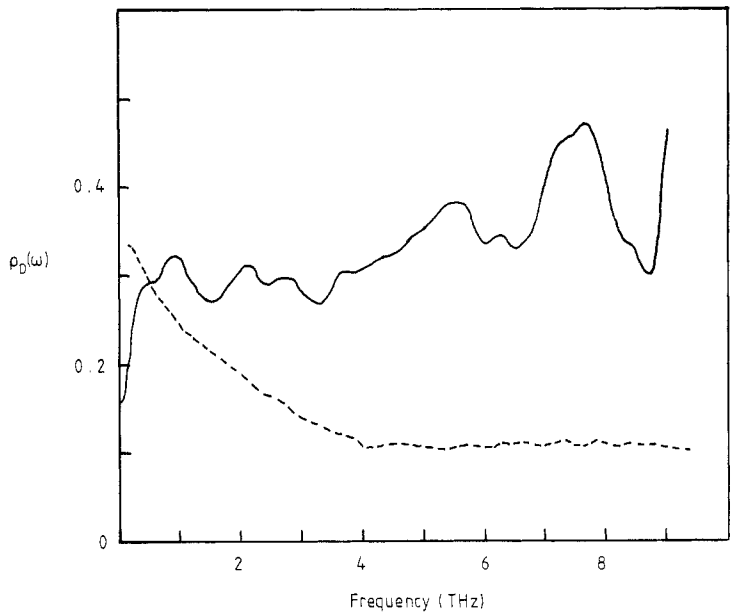

Figure 5. Frequency-dependent depolarisation ratio $\rho_D(\omega)$ from simulations of molten NaI at 973 K (broken curve), and from experiment of Raptis *et al* (1983) at 968 K (full curve).

Table 3. Time constants for spectral lineshapes. The time constants, as defined in (16), for the high-frequency exponential decay of the polarised and depolarised spectra for the simulation and the experiment of Raptis *et al* (1983).

	Simulation	Raptis *et al* (1983)
$I_\parallel : \tau_\infty$	0.6 ps	0.64 ps
$I_\perp : \tau_\infty$	0.5 ps	0.64 ps

behaviour in the simulation data is anomalous; this is due to the unfiltered 'bump' in the depolarised spectrum at low frequency (figure 2). The entry for $\rho_D(0)$ in table 2 is based on extrapolation of higher frequency data back to $\omega = 0$. The high-frequency (>7 THz) behaviour for the simulation is also anomalous; numerical problems in taking the ratio of small numbers may be to blame. The values of $\rho_D(\infty)$ in table 2 ignore this region.

3.5. Spectral lineshapes and time constants

The lineshapes are described by time constants for the exponential decay of the spectra, as in (16). A single exponential dominates the behaviour from about 1 THz onwards in both the polarised and depolarised simulated spectra. The lineshape below 1 THz lacks detail due to the statistics of the simulation and should not be regarded as accurate. There is a very weak shoulder and consequent change in slope in the simulated polarised spectrum at about 3 THz, but it is clearly not as strong as in the experimental spectrum (figure 2).

The time constants governing the high-frequency decay of the exponential intensity lineshapes are compared in table 3 for the simulations and the experiments of Raptis *et al* (1983).

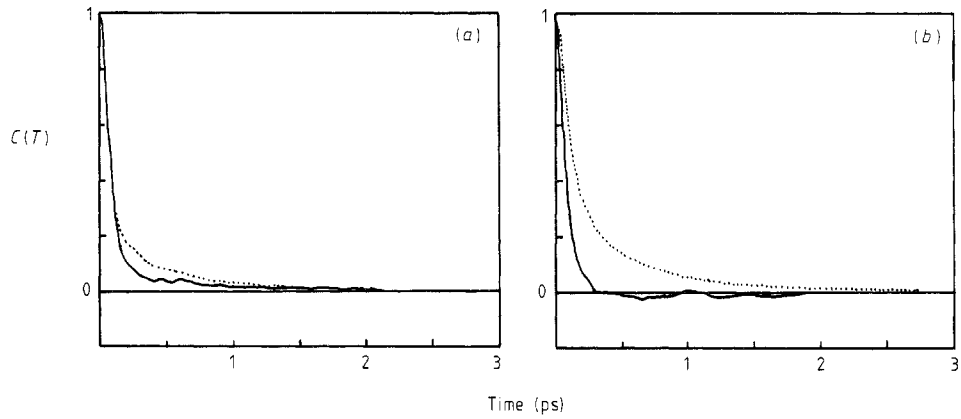

Figure 6. Time-domain scattering picture. The polarised (*a*) and depolarised (*b*) experimental spectra (figure 2) have been back-Fourier transformed to give the dotted curves, which are compared with the back-transforms of the smoothed spectra from the simulation (full curves). The simulation curves should be compared with figure 3 to see the time domain effect of the smoothing operation.

4. Discussion

The model is capable of reproducing the lineshape and relative intensity of the polarised and depolarised scattering from molten NaI to an encouraging extent. The first conclusion is that the instantaneous dipole moments as provided by shell model simulations are indeed fairly good representations of the 'real' ionic dipole moments.

The depolarisation ratios given by the model calculation are significantly lower than the completely anisotropic scattering value of 0.75, but they are not low enough to match experiment. The low frequency $\rho_D(0)$ is not too far off, but the lack of the experimentally observed shoulder in the polarised spectrum prevents the value from coming down to the observed high-frequency value of about 0.1. The simulated polarised and depolarised spectra in fact converge slightly, resulting in a rise of $\rho_D(\omega)$ with frequency.

The high-frequency depolarised lineshape, as characterised by the time constant τ_∞ is in quite good agreement with experiment; the mid-frequency region is less satisfactory, and the statistics are poor on the low-frequency region. The polarised lineshape is significantly wrong.

Figure 6 gives the time domain picture of the scattering lineshape. The experimental spectra have been back-transformed to the time domain, as have the *smoothed* spectra from the simulation. The simulation curves should be compared with the original time correlation functions for the simulation in figure 3 to see the effect in the time domain of the filtering operation. For the polarised correlations (figure 6(*a*)), the short-time behaviour of the two is in good agreement; the initial decay of the two curves is nearly identical. This is the time domain equivalent of the good high-frequency agreement of the corresponding spectra in figure 2. The lack of good agreement between about 0.2 and 0.5 ps is consistent with the failure to observe the mid-frequency shoulder in the simulation spectra. The agreement for the depolarised curves (figure 6(*b*)) is much worse, reflecting the divergence of the simulation and experimental depolarised spectra in figure 2 and table 3.

To understand these spectra further, the timescales of various processes in the NaI simulations are given in table 4. The characteristic decay times of vibrational, optical, and diffusive processes are calculated from our simulations as in Dixon and Sangster

Table 4. Timescales of processes in simulation of NaI melt. The first two rows gives the characteristic relaxation time (to e^{-1}) of the initial value of the velocity autocorrelation function for cations and anions, reflecting the timescale of phonon-like vibrational processes. The third row gives the relaxation time fo the dipole–dipole correlation function, which is related to infrared absorption. The last two rows (from Dixon and Sangster 1976) give the diffusion times (time to diffuse one near-neighbour spacing) for cations and anions.

Process	time (ps)
$\Sigma_i{}^+ m_i\langle v_i(0)\mathrm{v}_i(t)\rangle$	0.07
$\Sigma_i{}^- m_i\langle v_i(0)\mathrm{v}_i(t)\rangle$	0.07
$\langle(\Sigma_i u_i(0))(\Sigma_j \mu_j(t))\rangle$	0.21
τ_d^+	1.9
τ_d^-	2.8

(1976).

Diffusive processes are apparently too slow to be of much importance to the light scattering, except perhaps at very low frequency, where the experimental lineshape time constant goes up to about 1.6 ps for depolarised scattering (Raptis *et al* 1983), and the simulation results are inconclusive. The vibrational processes, however, have a characteristic decay time which is much too fast to account for that observed in the scattering processes.

It is interesting to note that the dipole–dipole correlation function relaxation time (table 4) is roughly equal to the known plasma period of molten NaI of 0.20 ps without polarisation effects and 0.28 ps with polarisation included (Raptis *et al* 1983).

These results indicate that the dipole–induced-dipole contributions to the scattering calculated here are important but are insufficient to describe the scattering completely. Specifically, no account has been taken here of the variation of an ion's polarisability as its local environment fluctuates in the melt. Short-range forces acting between ions will distort their electronic structure and alter their polarisability. Madden and Board (1987) have shown that there is significant interference between these short range effects and the DID terms. A future calculation should combine the superior dynamics of the shell model as used here with the more detailed polarisability variation models used by Madden and Board (1987), perhaps by designing a shell model potential whose shell parameters vary dynamically with environmental fluctuations.

From the computational viewpoint, one cause for some concern is the shell relaxation procedure, which implements the adiabatic approximation for the electron shell within the shell model. At each timestep, the electron shells are self-consistently relaxed to a position of no net force (Dixon and Sangster 1976). The relaxed shell position may or may not represent satisfactorily the dipole moment of a given ion at a given timestep; a more reasonable method for relaxing the shell positions is being sought.

Acknowledgments

We acknowledge the support of the SERC (UK), which provided grants of computer time at the Rutherford Appleton Laboratory for this work. One of us (JAB) thanks the Rhodes Trust for the award of a scholarship. We also thank Professor E W J Mitchell and Dr P A Madden and Dr R L McGreevy for useful discussions.

References

Bilz H, Strauch D and Wehner R K 1984 *Encyclopedia of Physics* vol XXV/2d *Light and Matter* Id, ed. L Genzel (Berlin: Springer)

Birman J L 1974 *Encyclopedia of Physics* vol XXV/2b *Light and Matter* Ib, ed. L Genzel (Berlin: Springer)
Bruce A D 1972 *J. Phys. C: Solid State Phys.* **5** 2909
Bruce A D and Cowley R A 1972 *J. Phys. C: Solid State Phys.* **5** 595
Ciccotti G and Hoover W eds 1987 *Proc. Int. School of Physics 'Enrico Fermi' 1985 (Varenna, Italy)* (Amsterdam: North-Holland)
Clarke J H R 1978 *Advances in Infrared and Raman Spectroscopy* vol 4, ed. R J H Clark and R E Hester (London: Heyden) p 109
Cochran W and Cowley R A 1967 *Encyclopedia of Physics* vol XXV/2a *Light and Matter* Ia, ed. L Genzel (Berlin: Springer)
Dixon M 1983a *Phil. Mag.* B **47** 509
—— 1983b *Phil. Mag.* B **47** 531
—— 1983c *Phil. Mag.* B **48** 13
Dixon M and Sangster M J L 1975 *J. Phys. C: Solid State Phys.* **8** L8
—— 1976 *J. Phys. C: Solid State Phys.* **9** 909
Elliott R J and Dixon M 1981 *J. Physique Coll.* **42** C6 175
Elliott R J, Krumhansl J A and Leath P L 1974 *Rev. Mod. Phys.* **46** 465
Fairbanks M, McGreevy R L and Mitchell E W J 1986 *J. Phys. C: Solid State Phys.* **19** L53
Giergiel J, Subbaswamy K R and Eklund P C 1984 *Phys. Rev.* B **29** 3490
Hoover W G 1986 *Molecular Dynamics, Springer Lecture Notes in Physics Series* vol 258 (Berlin: Springer)
Karo A M and Hardy J R 1966 *Phys. Rev.* **141** 696
Madden P A and Board J A 1987 *J. Chem. Soc., Faraday Trans.* II **83** 1891
McGreevy R L 1987 *J. Chem. Soc., Faraday Trans.* II **83** 1875
Mitchell E W J and Raptis C 1983 *J. Phys. C: Solid State Phys.* **16** 2973
Placzek G 1934 *Handbuch der Radiologie* VI 2, ed. E Marx (Leipzig: Akademische Verlag); (Engl. Transl. *University of California Radiation Lab. (UCRL) Translation No 526(L)*)
Raptis C, Bunten R A J and Mitchell E W J 1983 *J. Phys. C: Solid State Phys.* **16** 5351
Sangster M J L and Dixon M 1976 *Adv. Phys.* **25** 247